1.E.1:
2.G

Nuclear Physics A302 (1978) 186–204;

LEVELS OF ^{52}Fe STUDIED WITH THE (p, t) REACTION †

P. DECOWSKI ††, W. BENENSON, B. A. BROWN and H. NANN

Cyclotron Laboratory and Physics Department, Michigan State University, East Lansing, Michigan 48824

Received 28 December 1976
(Revised 2 March 1978)

Abstract: The ^{54}Fe(p, t)^{52}Fe reaction at 45 MeV has been used to study states of ^{52}Fe. Characteristic L-transfers in the angular distributions were used to assign $\approx$ 40 spins and parities. An $f_{7/2}$ shell model, with admixtures calculated in first-order perturbation theory, successfully accounts for both the location and strength of many of the observed levels.

E | NUCLEAR REACTIONS ^{54}Fe(p, t), E = 45 MeV; measured $\sigma(E_t, \theta)$. ^{52}Fe deduced levels, L, J, π. Enriched target, magnetic spectrograph. Shell model calculation.

1. Introduction

Studies of the ^{52}Fe nucleus are important for understanding nuclear structure in the upper part of the $f_{\frac{7}{2}}$ shell. The structure of this nucleus has been investigated in the past with the (^{3}He, n) [refs. [1,2])] and (p, t) reactions [3–6]). Spins and parities were assigned only to the most strongly excited states, which are characterized mainly by L = 0, 2 and 4 angular momentum transfers. Many of the weaker states remained unassigned, and there existed several controversies concerning even the stronger states.

The present high resolution experiment permits the finding of spins and parities for about forty levels with excitation energies up to 10 MeV. The comparison of the measured cross sections with the DWBA calculations provide some information about the distribution of $f_{\frac{7}{2}}^{-2}$ strength among the states. Admixtures of other orbitals which would drastically affect the cross section especially for L = 0 are accounted for by a first-order perturbation theory calculation.

2. Experiment

A beam of protons accelerated to an energy of 45 MeV by the Michigan State University Cyclotron bombarded a 250 μg/cm^2 target of ^{54}Fe enriched to 96.7%, which was deposited on 20 μg/cm^2 ^{12}C foil. The position of triton groups on the

† Work supported in part by the National Science Foundation.
†† On leave from the Institute of Experimental Physics of the University of Warsaw.

focal plane of an Enge split-pole spectrograph was measured by a delay-line counter [7]) backed with proportional and scintillation counters which provided energy loss and time-of-flight measurements for discrimination against other particles. The average resolution (FWHM) was $\approx$ 15 keV. The length of the position sensitive counter (25 cm) corresponded to $\approx$ 5 MeV interval in excitation energy.

The angular distributions were measured in the 6°–60° angular range in 2° steps at forward angles, and 3°–5° steps at more backward angles. For each angle the target was exposed to the beam for a total charge of 1–10 mC.

3. Results

The spectrum of tritons measured at 14° is shown in fig. 1. The only impurities present come from carbon, oxygen, and the 2.3 % admixture of ^{56}Fe in the target. The intensities of the peaks were extracted from measured spectra by a fitting procedure which used experimental line shapes derived from the most intense peaks. The cross sections were obtained by normalizing measured yield to the yield of protons elastically scattered from the same target. The elastic scattering cross section was calculated with typical proton optical model parameters [8]). The resulting target thickness agreed with α-particle energy loss measurements to within 15 %.

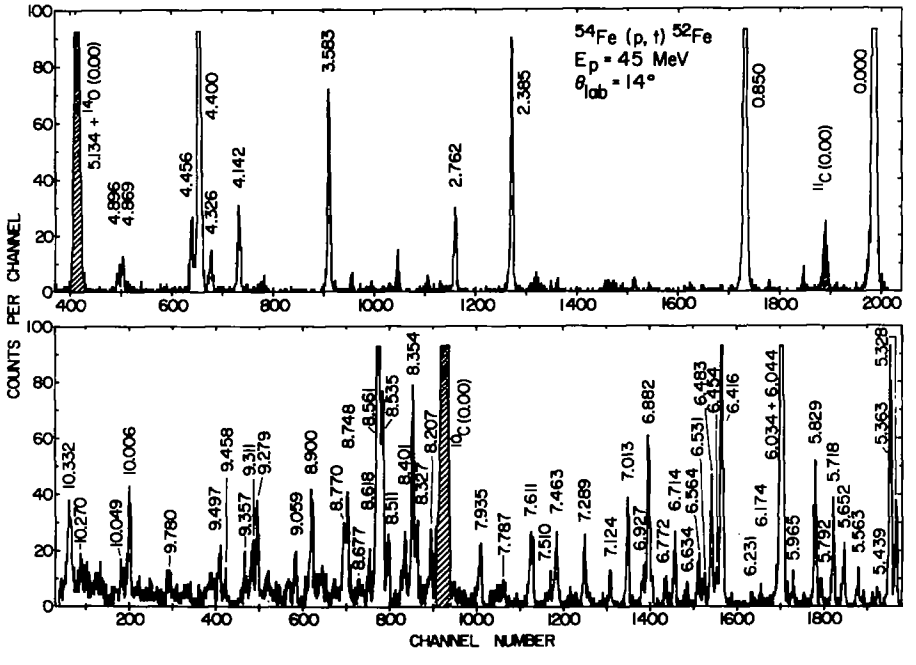

Fig. 1. Spectrum of tritons at 14°.

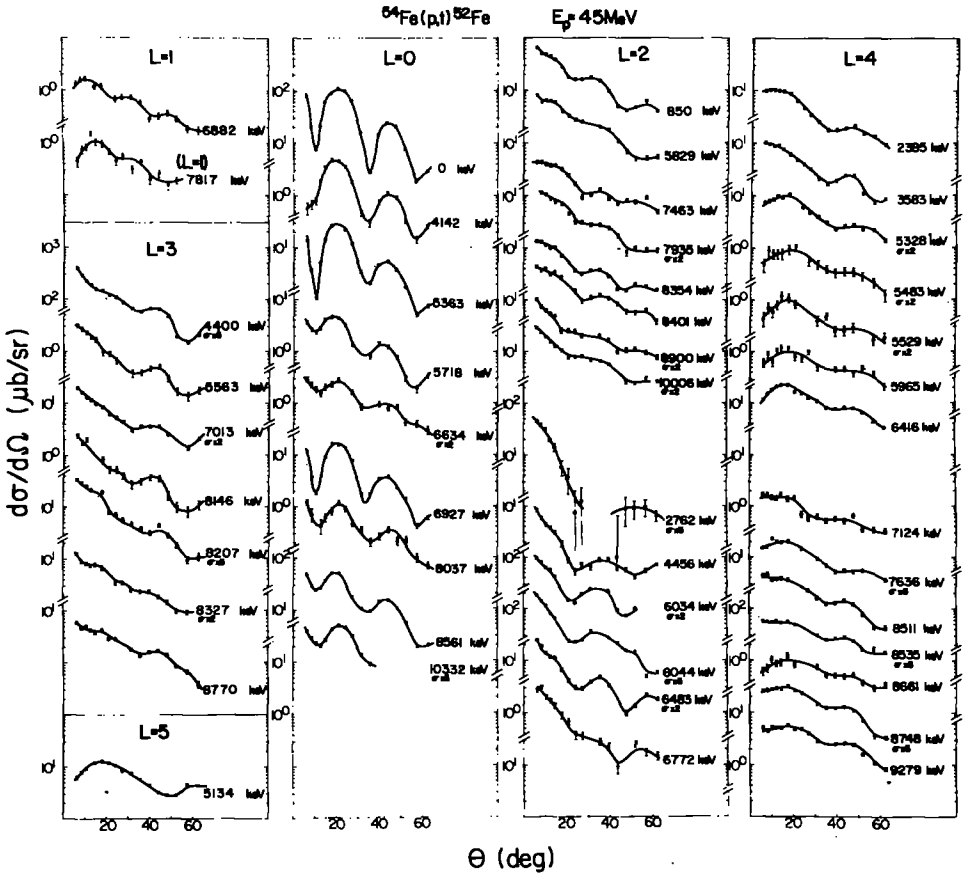

Fig. 2. Angular distributions of tritons from the ^{54}Fe(p, t)^{52}Fe reaction. Lines are drawn to guide the eye.

The measured angular distributions are shown in figs. 2 and 3. They exhibit features prominent enough to make a distinction between different L-transfers for all the stronger states. One step two-neutron pickup excites only natural parity states (assuming the transfered neutron pair is in a $S = 0$ configuration), and since the target is 0^+, it was possible to infer spins and parities of the observed states from the L-transfer. They are listed together with excitation energies in table 1.

The measured excitation energies are free from the error connected with the non-linearities of the delay-line counter. This was achieved by calibrating the counter using the positions of the triton group corresponding to the ground state of ^{10}C at many different settings of the spectrograph magnetic field. The isospin assignments in table 1 are based on the correspondence to the parent nuclei, ^{52}Mn for $T = 1$ and ^{52}Cr for $T = 2$. For ^{52}Mn this included a comparison to the strength and angular distribution of the L-transfer observed in the ^{54}Fe(p, ^{3}He) reaction [9]).

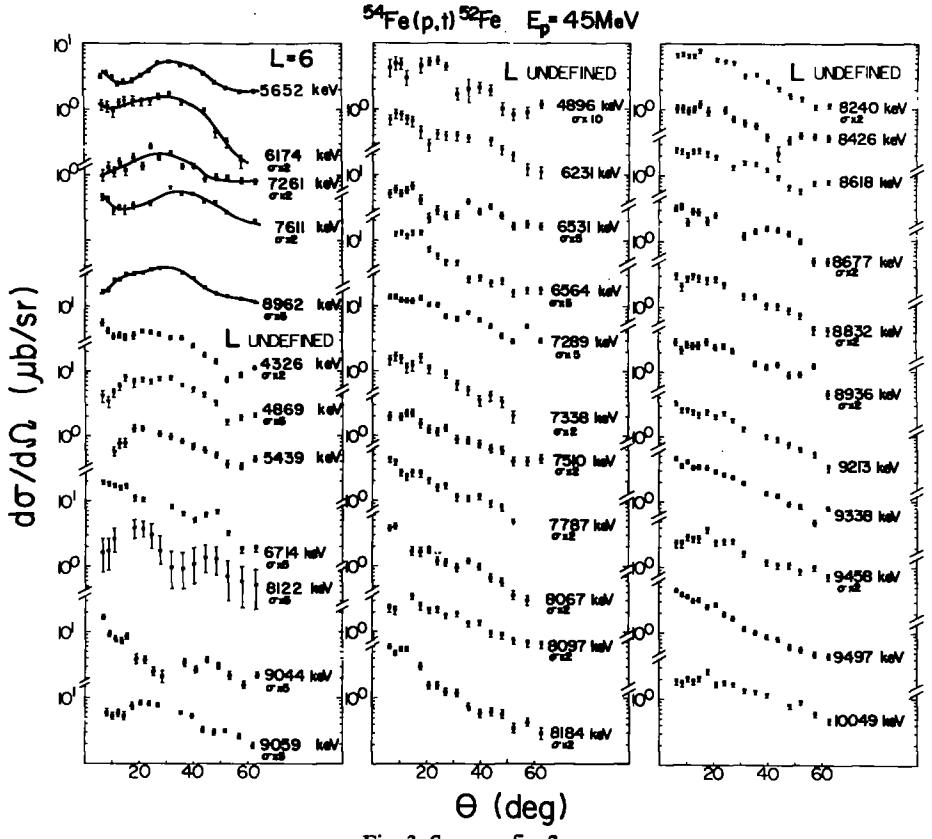

Fig. 3. Same as fig. 2.

The identification of L-transfer values was based mainly on systematics of the slope and the positions of the minima and maxima of the angular distributions. The angles corresponding to minima and maxima were determined by comparison to the line representing the average slope of the differential cross section on a logarithmic scale. The average slope appeared to be approximately a linear function of L and changed from $\approx$ 1.5 decades per 60° for $L = 0$ to $\approx$ 0.65 decades per 60° for $L = 6$. This procedure enhanced less-pronounced minima and maxima and helped to localize them for all L-transfers in a systematic way. The positions of minima and maxima for all identified L-transfers are shown in fig. 4. They group around values which follow a well-defined systematic trend. The scatter of values represents the errors in the measurements (especially important for flat and weak extrema) and the differences in shape of individual angular distributions for a given L-transfer. As in any spin assignments with direct reactions, there are many effects which can lead to mis-identification. These include unresolved multiple states in the same peak, extreme

TABLE 1

Excitation energies and spin-parity assignments for levels of ^{52}Fe

(p, t), E_p = 45 MeV [a]				(p, t), E_p = 40 MeV [b]		(^{3}He, n), $E_{^3He}$ = 13 MeV [c]	
E_x (keV)	J^π		$\frac{\sigma_{int}}{2\pi}$ (μb)	E_x (MeV)	J^π	E_x (MeV)	J^π
0	0^+		13.4	0.0	0^+	0.0	0^+
850± 5	2^+		6.0	0.84	2^+	0.84	2^+
2385± 5	4^+		1.5	2.36	4^+	2.36	4^+
2762± 5	(2^+)		0.27	2.74		2.75	2^+
3583± 5	4^+		1.3	3.55	2^+	3.59	4^+
4142±10	0^+		0.57	4.14	0^+	4.16	0^+
4326± 8			0.55				
4400± 5	3^-		6.7	4.36	4^+	4.43	2^+
4456± 8	2^+		0.44				
4869±15			0.44	4.86	(5^-)		
4896±15			0.11				
5134± 8	5^-		2.7	5.11	(3^-)		
5328± 8	4^+		0.92				
5363± 5	0^+		3.1	5.31	0^+	5.36	0^+
5439±15			0.32				
5483±20	4^+		0.11				
5529±20	4^+		0.10				
5563± 8	(3^-)		0.25				
5652± 8	6^+	$T = 1$	1.6	5.65	6^+		
5718± 8	0^+		0.66			5.76	0^+
5792±10			0.48	5.79			
5829± 5	2^+		0.88			5.82	2^+
5965±15	4^+		0.26				
6034± 5	2^+	$T = 1$	3.9	6.02	4^+	6.07	(2^+)
6044± 5	2^+		2.6				
6174±15	(6^+)		0.23				
6231±15			0.15				
6416± 5	4^+	$T = 1$	4.7	6.38	5^-		
6454±15			0.49				
6483± 5	2^+		0.85			6.52	3^-
6531±10			0.27				
6564± 8			0.39				
6634±10	(0^+)		0.25				
						6.70	2^+
6714± 8			0.65	6.67	2^+		
6744±15							
6772± 8	(2^+)		0.19				
6882± 5	1^-		0.25				
6927±15	0^+		2.0	6.84	0^+		
7013± 5	3^-		0.95	6.98			
7124±10	(4^+)		0.31			7.12	
7261±15	(6^+)		0.32				
7289± 8			0.61	7.24		7.28	
7338±10			0.13				
7463± 8	2^+		0.60	7.42		7.47	2^+
7510±15			0.20				
7611±10	6^+	$T = 1$	0.84				

TABLE 1 (continued)

(p, t), E_p = 45 MeV [a]				(p, t), E_p = 40 MeV [b]		(^{3}He, n), $E_{^3He}$ = 13 MeV [c]	
E_x (keV)	J^π		$\frac{\sigma_{int}}{2\pi}$ (μb)	E_x (MeV)	J^π	E_x (MeV)	J^π
7636±15	4^+	$T = 1$	0.73	7.58		7.64	
7787±10			0.26				
7817±15			0.16			7.82	
7935±10	2^+		0.60				
8037±15	0^+		0.17			8.05	0^+
8067± 8			0.23				
8097±10			0.32				
8122±15			0.13				
8146±10	3^-		0.18				
8184±10			0.27				
8207± 8	(3^-)		0.54				
8240±10			0.72				
8327±10	(3^-)		0.64				
8354± 5	2^+	($T = 1$)	1.6	8.33	(4^+)	8.36	2^+
8401± 8	2^+		0.55				
8425±15			0.25				
8461±10							
8511± 8	4^+		0.76				
8535± 5	4^+		2.7				
8561± 5 [d]	0^+	$T = 2$	7.3	8.52	0^+	8.57	0^+
8618± 8			0.55				
8661±15	(4^+)		0.27				
8677±10			0.34				
8727±15							
8748±10	4^+	($T = 1$)	1.3				
8770±10	(3^-)		0.87				
8832±10			0.31				
8872±10							
8900± 8	(2^+)		0.44				
8936±10			0.35				
8962±10 [e]	(6^+)	($T = 1$)	2.2	8.92			
8985±10							
9044±15			0.29			9.01	2^+
9059±15			0.46				
						9.13	
9213± 8			0.56				
9279± 8	4^+		1.3	9.26		9.25	
9311± 8							
9338±10			0.76				
9357±15							
9458±10			0.36				
9497± 8			0.57			9.47	
						9.77	
10006± 5	(2^+)	($T = 2$)	1.4	9.99	2^+		
10049±10			0.56			10.06	2^+
10332± 5	0^+		1.5			10.31	0^+

[a]) Present experiment. [b]) Ref. [3]). [c]) Ref. [1]).
[d]) Doublet of two 0^+ levels separated by ≈ 4 keV.
[e]) Level with probable multiplet structure.

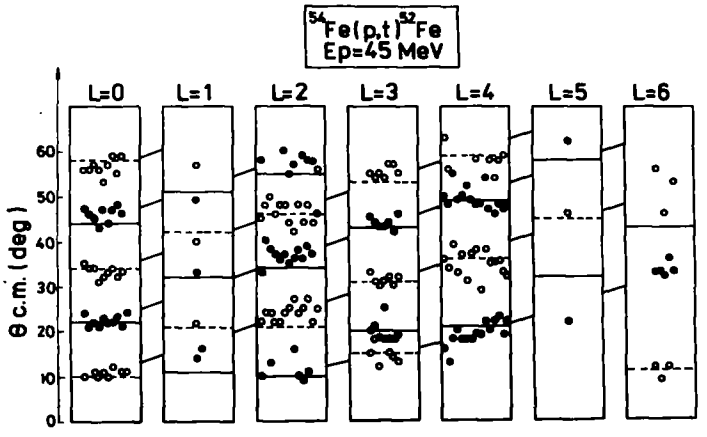

Fig. 4. The positions of maxima and minima in the experimental differential cross sections (full and open circles, respectively) and in the DWBA calculations (solid and dotted lines). For each L-value they are ordered with increasing excitation energy from left to right.

statistical fluctuations at the crucial angles and strong two-step contributions disturbing the shape of the angular distribution. Many states have their spin assignments bracketed because distinct features of the angular distribution do not conform exactly to those of any L-transfer. Within the framework of the systematics described above and the assumption of a direct single-step process, each assignment is really a best estimate of the spin, and the bracket indicates a very weak distinction from other L-transfers.

It is seen from fig. 4 that it is not always possible to distinguish unambiguously between neighboring L-values if the distinction is limited to analysis of the positions of local extrema. This is the case in a comparison of $L = 1$ to $L = 2$ and $L = 3$ to $L = 4$ transitions. Fortunately in this situation there are well-pronounced differences at forward angles which in most cases are able to remove the ambiguities. The differential cross sections for $L = 1$ transitions drop down at angles less than 10° whereas $L = 2$ transitions exhibit the opposite trend. A similar situation exists in the case of $L = 4$ and 3 transitions. These trends at forward angles are also well described by DWBA calculations (see figs. 5 and 6).

3.1. THE $L = 0$ TRANSITIONS

The prominent oscillatory character of the angular distributions for these transitions allows one to distinguish them unambiguously from other transitions. Nine transitions were identified as $L = 0$ in the excitation region investigated. The strongest ones lead to the ground state and to the 0^+, $T = 2$ state found in earlier works near 8.5 MeV [refs. [1-4,6])]. The present experiment shows that in fact the 0^+, $T = 2$

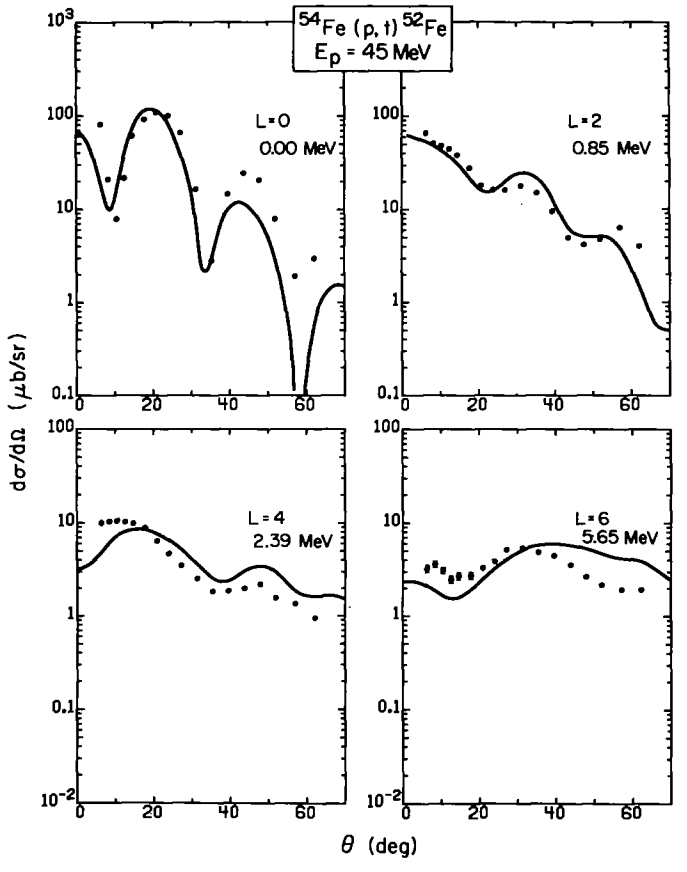

Fig. 5. Examples of DWBA fits to experimental angular distributions for even-L transfers.

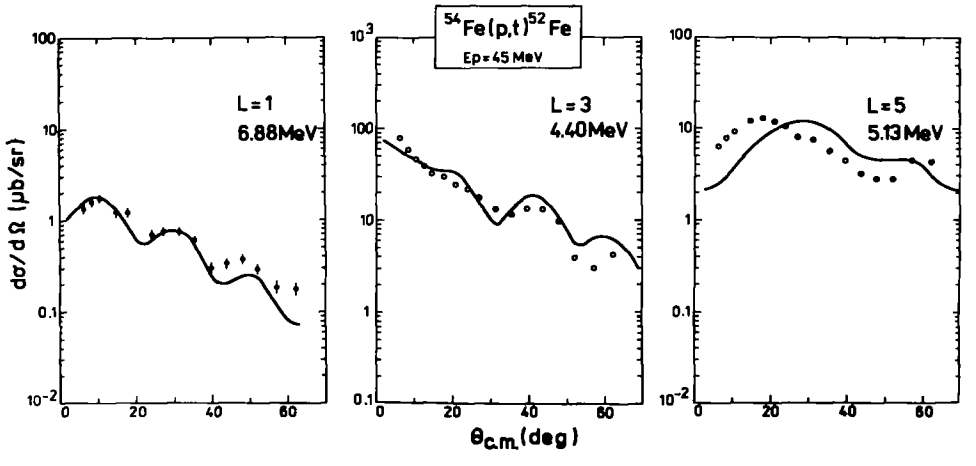

Fig. 6. Examples of DWBA fits to experimental angular distributions for odd-L transfers.

state is split into two states separated by about 4 keV but the energy resolution was not good enough to measure both angular distributions separately. Such splitting is a common occurrence for nuclei in the $f_{\frac{7}{2}}$ shell [10]).

3.2. THE $L = 2$ TRANSITIONS

There are two types of shapes of $L = 2$ transitions which differ at forward angles. They are grouped in fig. 2. The strongest transitions excite the first 2^+, $T = 0$ state and the first 2^+, $T = 1$ state, which again appears to be split into two states 10 ± 1 keV apart. In ref. [3]), an assignment $J^\pi = 4^+$ was made for a state at 6.02 MeV as well as for a state at 8.33 MeV and is therefore in contradiction with the present work.

Direct measurement of the angular distribution of the 2.762 MeV state was not possible because it was obscured by tritons from the ^{54}Fe 6.325 MeV, 3^- state which is strongly excited in the (p, t) reaction on the ^{56}Fe admixture in the target. The extraction of this contribution is based on the measured cross section for the ^{56}Fe(p, t)^{54}Fe reaction at the same energy [11]) and yielded an $L = (2)$ angular distribution in agreement with the 2^+ assignment for this state in ref. [1]).

3.3. THE $L = 4$ TRANSITIONS

As was mentioned above the angular distribution for $L = 4$ and $L = 3$ transitions often are quite similar, and it is necessary to be very careful in the identification. The strongest $L = 4$ transition is to the 4^+, $T = 1$ state at 6.416 MeV. Ref. [3]) identified this state at 5^-. The difference between experimental angular distributions for $L = 4$ and $L = 5$ transitions measured in the present experiment is large enough to rule out this possibility. Our assignment of spin and parity 4^+ for the state at 3.583 MeV does not agree with the 2^+ assignments of ref. [3]), but it does agree with the result of ref. [1]).

3.4. THE $L = 6$ TRANSITIONS

The main feature of these transitions is peaking around 30°. The strongest transitions lead to the analog of the ^{52}Mn, 6^+, $T = 1$ ground state at 5.652 MeV and to the 6^+, $T = 1$ state at 7.611 MeV. The angular distribution of the strong transition to the state at 8.962 MeV has a shape which suggests an admixture of another L-value (probably 4 or 5) from an unresolved nearby state. Because of the lack of a distinct signature, it is probable several strong $L = 6$ states were missed.

3.5. THE ODD-L TRANSITIONS

One of the most strongly excited states is at 4.400 MeV with an $L = 3$ angular

distribution. In previous (p, t) work [3]) this state was identified as 4^+. The strong excitation of this state and its low energy suggest that it is the collective octupole vibration which occurs in all f-p shell nuclei around this energy. The lack of a steep rise at forward angles makes an $L = 3$ assignment for the 5.56 MeV state tentative.

One 5^- state was observed at 5.134 MeV; in ref. [3]) it was tentatively identified as 3^-

4. DWBA analysis and discussion

Up to the present, a theory which can account for all states observed in ^{52}Fe has not been attempted. However, calculations assuming $1f_{\frac{7}{2}}^{-4}$ configurations which account for many of the positive parity levels have been carried out [14]). Since the excitation energies and electromagnetic transition strengths for many of the levels in ^{54}Fe and ^{52}Fe seem to be well described by the $f_{\frac{7}{2}}^n$ wave functions [15,16]), DWBA calculations for positive parity states were performed with the zero-range code DWUCK under the assumption of pure $f_{\frac{7}{2}}$ two-neutron pickup. As will be discussed below the pickup strength is strongly enhanced by the coherent contributions of many orbitals, especially for $L = 0$. However, the dominant effect of these contributions can be treated as an overall enhancement factor since the amplitudes for configurations outside the $f_{\frac{7}{2}}$ shell are small (and hence perturbation theory can be applied) and since the DWBA angular distributions are insensitive to the particular orbits involved in the two-neutron pickup.

The optical model parameters listed in table 2 were the same as used in ref. [12]). Examples of DWBA fits with pure $f_{\frac{7}{2}}^2$ pickup for positive parity states and $f_{\frac{7}{2}}d_{\frac{3}{2}}$ pickup for negative parity states are shown in figs. 5 and 6. The shapes of these calculated angular distributions depend very little on the details of the radial form factors. They are mainly determined by the distorted waves in the entrance and exit channels.

Zero-range DWBA calculations were not able to produce good fits to the shapes of the experimental $L = 5$ and 6 angular distributions. As can be seen from fig. 4 the position of the first maximum for these transitions systematically deviates from experimental values. This leads to a problem in evaluating the 6^+ strengths, as will be discussed below.

TABLE 2

Optical potential and neutron bound state well parameters used in the DWBA calculations

V	V_0 (MeV)	r_0 (fm)	a_0 (fm)	W (MeV)	W_D (MeV)	r' (fm)	a' (fm)	r_c (fm)	λ^a)
protons	47.5	1.20	0.70		13.0	1.25	0.70	1.25	
tritons	173.9	1.15	0.72	20.6		1.50	0.82	1.40	
bound neutron	V^b)	1.25	0.65						25

a) Thomas spin-orbit factor.

b) Fitted to a neutron binding energy equal to $\frac{1}{2}(B_{2n}^{*} + E_x)$.

The experimental cross sections were compared with DWUCK cross sections using the formula:

$$\sigma_{exp} = 9.72(\varepsilon D_0^2)(S^{\frac{1}{2}})^2(2J+1)^{-1}\sigma_{DWUCK},$$

where σ_{exp} and σ_{DWUCK} are the experimental and DWBA cross sections integrated over the angular interval 6°–60°. The constant 9.72 accounts for the details of the triton wave function and the range of the interaction [13]), whereas εD_0^2 is a normalization factor which will be discussed later. The spectroscopic amplitude, $S^{\frac{1}{2}}$, in the case of pickup of two neutrons coupled to spin J from a filled shell, is $(2J+1)^{\frac{1}{2}}a$. The quantity a^2 is the probability of the $(f_{\frac{7}{2}}^{-2})_J$ neutron configuration in the final state.

Thus, for each level a multiplicative factor $\varepsilon D_0^2 a^2$ was extracted from the DWBA analysis. The relative values of a^2 were compared with the predictions of a $f_{\frac{7}{2}}^n$ shell-model calculation by normalizing εD_0^2 to the state which should carry the most pure

TABLE 3

Normalization factors used in the DWBA analysis and calculated enhancement factors

J^π	εD_0^2 exp	fp orbitals		sd-fp-$g_{9/2}$ orbitals	
		ε	D_0^2 [c])	ε	D_0^2 [c])
0^+	93 [a])	2.16	43	4.33	21
2^+	44 [a])	1.49	30	2.26	19
4^+	22 [a])	1.10	20	1.32	16
6^+	16 [b])	1.00	16	1.03	16

[a]) From a comparison of integrated cross section between 6° and 60° to the DWBA cross sections for selected states (see text).

[b]) The experimental and DWBA cross sections corresponding to the 5.65 MeV state were normalized at 30°.

[c]) In units of 10^4 MeV^2 · fm^3.

TABLE 4

Comparison of experimental strength with theoretical $f_{7/2}^{-2}$ strength for 0^+ levels

	Experiment			Theory	
	E_x (MeV)	a^2	$\sum a^2$	E_x (MeV)	a^2
$T = 0$	0.00	0.510		0.00	0.558
	4.14	0.018	0.227	7.53	0.181
	5.36	0.106			
	5.72	0.021			
	6.63	0.007			
	6.93	0.068			
	8.04	0.007			
	10.33	0.050		10.92	0.011
total		0.788			0.750
$T = 2$	8.56	0.250		8.06	0.250

TABLE 5

Same as table 4 for 2^+ levels

	Experiment			Theory	
	E_x (MeV)	a^2	$\sum a^2$	E_x (MeV)	a^2
	0.85	0.277		1.05	0.354
	(2.76	0.013)			
	4.46	0.023			
	5.83	0.047		5.98	0.031
	6.48	0.045			
$T = 0$	(6.77	0.011)	0.263		
	7.46	0.033			
	7.93	0.034			
	8.40	0.032			
	(8.90	0.025)			
				9.47	0.003
				9.94	0.028
total		0.540			0.417
	6.03	0.207	0.343	5.51	0.343
	6.04	0.136			
$T = 1$	8.35	0.092		8.85	0.157
				10.37	0.000
total		0.435			0.500
$T = 2$	(10.01	0.083)		9.50	0.083
				11.35	0.000

$f_{\frac{7}{2}}^{-2}$ strength for each L-transfer. These were isolated, strongly excited states which correspond closely in excitation energy to calculated energies. The following states were chosen; 0^+, the $T = 2$, 8.56 MeV state; 2^+, the lowest $T = 1$, 6.03 MeV state; 4^+, the lowest $T = 1$ state at 6.42 MeV; 6^+, the lowest $T = 1$ state at 5.65 MeV. The experimental normalization factors εD_0^2 obtained this way for each spin are listed in the second column of table 3. The extracted pickup strengths are compared with the theoretical $f_{\frac{7}{2}}$ strengths a^2 in tables 4–7 and in fig. 7.

The $f_{\frac{7}{2}}^n$ calculations were carried out with the eight two-body matrix elements with $J = 0$–7 taken from the experimentally observed ^{54}Co energy levels which are thought to have predominantly $f_{\frac{7}{2}}^{-2}$ configurations [14]). These levels are 0, 937, 1446, 2278, 2630, 2151, 3085 and 199 keV for $J = 0$ through 7, respectively. With these matrix elements the $T_{\frac{1}{2}} = 56$ sec, isomeric 12^+ level in ^{52}Fe [ref. [15])] is predicted at 6.974 MeV compared with the observed energy of 6.83 ± 0.25 MeV. It also predicts correctly that the 10^+ state lies above the 12^+ state. The wave functions for ^{52}Fe were obtained in the proton-neutron coupling scheme in the form

$$|J_\alpha\rangle = \sum_{J_n J_p} a(J_p, J_n, J_\alpha)|j_p^{-2}(J_p) j_n^{-2}(J_n) J_\alpha\rangle,$$

TABLE 6

Same as table 4 for 4^+ levels

	Experiment			Theory	
	E_x (MeV)	a^2	$\sum a^2$	E_x (MeV)	a^2
	2.39	0.106	0.206	2.73	0.208
	3.58	0.100			
	5.33	0.079			
	5.48	0.010			
$T = 0$	5.53	0.008	0.149		
	5.97	0.023		5.87	0.170
	(7.12	0.029)			
				7.99	0.018
	8.51	0.079			
	8.54	0.279	0.532		
	(8.66	0.029)			
	9.28	0.145		9.92	0.021
				10.14	0.000
total		0.887			0.417
	6.42	0.424		6.07	0.424
	7.64	0.071		7.73	0.012
$T = 1$	8.75	0.137		10.16	0.042
				11.29	0.019
total		0.561			0.500
$T = 2$				10.45	0.000
				10.69	0.083

TABLE 7

Same as table 4 for 6^+ levels

	Experiment			Theory	
	E_x (MeV)	a^2	$\sum a^2$	E_x (MeV)	a^2
				4.33	0.207
				5.37	0.110
	(6.17	0.042)			
$T = 0$	(7.26	0.065)		7.82	0.070
				8.31	0.015
				11.11	0.016
total					0.417
	5.65	0.287		5.22	0.287
	7.61	0.177		7.79	0.146
$T = 1$	(8.96)			8.78	0.023
				11.19	0.043
total		0.464			0.500
$T = 2$				11.14	0.083

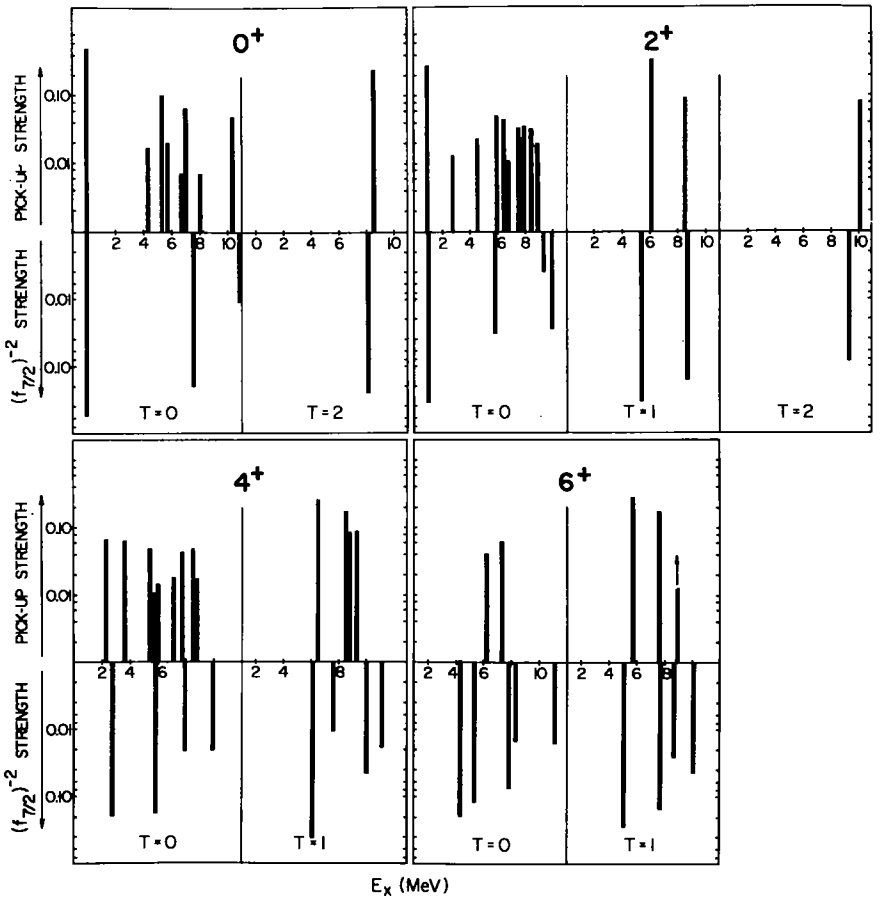

Fig. 7. The comparison of measured pickup strength with theoretically predicted $f_{7/2}^{-2}$ strength.

where α distinguishes states with the same J. The ^{54}Fe wave function is $|j_p^{-2}(J_p = 0)\rangle$ in this model. The (p, t) amplitudes are then just $[a(J_p = 0, J_n = J_\alpha = L, J_\alpha)]$.

The experimental and theoretical pickup strengths summed over all the 0^+ states given in table 4 are in good agreement. The strength of the theoretical state at 7.53 MeV appears to be divided among six additional states. This large number of 0^+ states can be accounted for by excited seniority-zero states as well as states originating from the seniority-four couplings of excited states in ^{54}Fe below 4 MeV. The importance of using an exact $f_{\frac{7}{2}}$ shell model as opposed to the simple pairing model [17]) or pure seniority $f_{\frac{7}{2}}$ model [13]) is shown by the ratio of the cross sections for the $T = 0$ ground-state to the $T = 2$, 8.56 MeV state. The latter models assume that the ^{52}Fe ground and $T = 2$, 0^+ state have pure seniority zero, in which case their cross section ratio is given by isospin Clebsch-Gordan coefficients to be 3.

In the exact $f_{\frac{7}{2}}$ calculation this ratio is 2.23 as compared with the experimental value of 2.04.

For $L = 2$ and 4 the lowest few states of each isospin are well reproduced both in energy and strength by the $f_{\frac{7}{2}}$ model. The strength of the $T = 0$, $L = 4$ and 6 transitions appears to be divided between two experimental levels for each spin the summed strength of which corresponds to the strength of a single level predicted in the $f_{\frac{7}{2}}$ model. This is just the situation which would be expected if the ground state of ^{54}Fe were predominantly $f_{\frac{7}{2}}^{-2}$ and the excited states in ^{52}Fe were $f_{\frac{7}{2}}^{-4}$ mixed with core excited configurations. In addition there is a large enhancement of $T = 0$ strength beyond the $f_{\frac{7}{2}}$ model in the region of 4–9 MeV especially for $L = 4$. This is indicative of a 1p-3h admixture in the ^{54}Fe ground state which would allow the direct population of excited states in ^{52}Fe via a $f_{\frac{7}{2}}p_{\frac{3}{2}}$ $L = 2, 4$ pickup or the pickup of two particles from the sd shell. The role of 2p-4h admixtures in ^{54}Fe will be discussed below.

The normalization factors εD_0^2 given in table 3 show a large variation with J. The large value of εD_0^2 for $J = 0$ indicates the enhanced probability of finding two neutrons in a relative 0s state at the nuclear surface. This enhancement can be found in the shell model when a large number of orbitals, at least all the orbitals in a major shell, are coherently mixed via a short-range attractive interaction. In its extreme this coherence leads to the BCS pairing model, a model which appears to work best, for example, in the Pb isotopes where most of the $J = 0$ sum rule limit is found in ground states [18]).

In the $f_{\frac{7}{2}}$ shell the $f_{\frac{7}{2}}^n$ component dominates the wave function and therefore the effect of the two-nucleon correlations can be estimated in perturbation theory. The situation for ^{54}Fe(p, t)^{52}Fe reaction is illustrated diagrammatically in fig. 8. Fig. 8a shows the zeroth-order process, which is the result of the two-neutron annihilation operator [19]) $M_J = -\sum_{j_n} (j_n+\frac{1}{2})^{\frac{1}{2}} A[(j_n^2)_J]$ acting on the initial state of two proton holes with $J_p = 0$ and a filled shell of neutrons. Fig. 8b represents the effect of the admixture of two neutron holes in the 1d-2s orbitals in the final state, and fig. 8c represents the admixture of two neutron particles in the 2p-1$f_{\frac{7}{2}}$-1$g_{\frac{9}{2}}$ orbitals in the

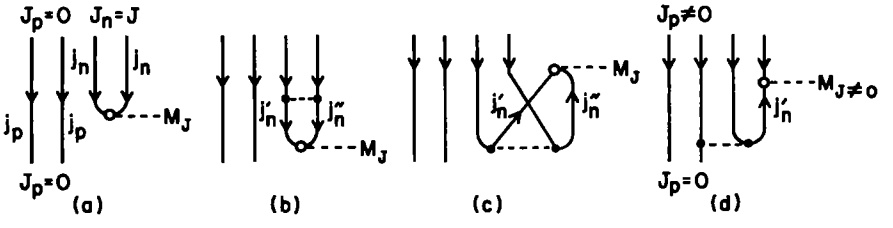

Fig. 8. Diagrams of the ^{54}Fe(p, t)^{52}Fe reaction assuming, (a) the zeroth-order process with ^{54}Fe in a pure $(j_p = 1f_{7/2})^{-2}_{J_p=0}$ configuration and ^{52}Fe in a pure $(j_p = 1f_{7/2})^{-2}_{J_p=0}(j_n = 1f_{7/2})^{-2}_{J_n=J}$ configuration, (b) a first-order process which includes two-hole admixtures in ^{52}Fe, and (c) a first-order process which includes two-particle admixtures in ^{54}Fe. Diagram (d) shows a first-order process due to three-hole one-particle admixtures with $(j_p = 1f_{7/2})^{-2}_{J_p\neq 0}$ in ^{54}Fe.

TABLE 8

Spectroscopic amplitudes and relative enhancement factors δ for the 2h and 2p admixtures in the ^{54}Fe(p, t)^{52}Fe reaction

J	$1d^2_{5/2}$	$2s^2_{1/2}$	$1d^2_{3/2}$	$1f^2_{7/2}$	$2p^2_{3/2}$	$1f^2_{5/2}$	$2p^2_{1/2}$	$1g^2_{9/2}$	$2s_{1/2}1d_{5/2}$	$2s_{1/2}1d_{3/2}$	$1d_{5/2}1d_{3/2}$	$2p_{3/2}1f_{5/2}$	$2p_{3/2}2p_{1/2}$	$2p_{1/2}1f_{5/2}$
							$S^{1/2}/(2J+1)^{1/2}$							
0^+	−0.152	−0.100	−0.225	1	0.141	0.192	0.065	−0.147						
2^+	−0.035		−0.049	1	0.031	0.045		−0.035	−0.042	−0.048	−0.032	0.017	0.034	0.026
4^+	−0.016			1		0.020		−0.018			−0.041	0.022		
6^+				1				−0.010						
							δ							
0^+	0.152	0.132	0.137	1	0.320	0.067	0.082	0.192						
2^+	0.035		0.028	1	0.068	0.016		0.046	0.085	0.069	0.019	0.013	0.094	0.031
4^+	0.015			1		0.007		0.022			0.063		0.044	
6^+				1				0.014						

initial state. The zeroth-order process gives $S^{\frac{1}{2}}(2J+1)^{-\frac{1}{2}} = 1$, and the amplitudes for the first-order processes (figs. 8b and c) are

$$\frac{S^{\frac{1}{2}}(j_n' j_n'')}{(2J+1)^{\frac{1}{2}}} = \frac{-\langle j_n^2 J|V|j_n' j_n'' J\rangle}{|\mathscr{E}(j_n')+\mathscr{E}(j_n'')-2\mathscr{E}(j_n)|} \tag{1}$$

These have been calculated with a delta function two-body interaction adjusted to give the $f_{\frac{7}{2}}^2$, $J = 0$–6 splitting of 3.085 MeV and with the single particle energies $\mathscr{E}$ appropriate for ^{56}Ni taken from Harvey and Khanna [20]). The results are given in table 8.

The enhancement factor ε was then calculated from the expression

$$\varepsilon = [1 + \sum_{j_n', j_n'' \neq j_n} \delta(j_n' j_n'')]^2,$$

where

$$\delta(j_n' j_n'') = \frac{S^{\frac{1}{2}}(j_n' j_n'')[\sigma_{\mathrm{DWUCK}}^{\max}(j_n' j_n'')]^{\frac{1}{2}}}{(2J+1)^{\frac{1}{2}}[\sigma_{\mathrm{DWUCK}}^{\max}(j_n^2 = f_{\frac{7}{2}}^2)]^{\frac{1}{2}}}. \tag{2}$$

The ratio of the square root of the DWUCK cross sections, including the appropriate phase factor, was obtained at an angle for a maximum in the angular distribution for each J; $\approx 20°$, $\approx 32°$, $\approx 17°$ and $\approx 38°$ for $J = 0$–6, respectively. This is justified because the ratios of the DWBA angular distributions are nearly independent of angle. In addition the ratios of the DWUCK cross sections are not very sensitive to the Q-value over the range of excitation energies studied [see fig. 1 in ref. [21])]. The values of $\delta(j_n' j_n'')$ are given in table 8, and the enhancement factor ε is given in table 3.

From fig. 8 one can see that the effect of the first-order diagrams 8b and 8c is simply to renormalize the two-neutron transfer operator by a factor ε which is independent of the detailed $f_{\frac{7}{2}}^n$ configurations involved. That is, except for the small Q-value dependence in δ and the single particle energy dependence in eq. (1), the *same* value of ε should describe all two-neutron transfer processes in the $f_{\frac{7}{2}}$ shell. This renormalization effect has been found experimentally for the (t, p) reactions on the Ca isotopes [22]).

Even though the probabilities of the core-excited components are quite small (16.6 % and 1.5 % for $J = 0$ and 2, respectively), ε is very large especially for $L = 0$ because the contributions are all coherent, and many of the configurations for example $(2s_{\frac{1}{2}})^2$ and $(2p_{\frac{1}{2}})^2$ have a large component of 0s relative motion. The monopole pairing is predominent, but there is also a large quadrupole pairing enhancement.

There are several first-order and many higher-order diagrams which cannot be considered as a renormalization of the $f_{\frac{7}{2}}^n$ amplitudes, but their effects are probably much less important than the ones discussed above. An example is fig. 8d which shows particles which are picked up from the $1f_{\frac{7}{2}}$ and $2p_{\frac{3}{2}}$ orbitals leaving ^{52}Fe in a state with the two protons in a 2^+ or 4^+ configurations. This diagram represents the (p, t) reaction amplitude due to the ^{54}Fe, $f_{\frac{7}{2}}^{-2}$ 2^+ or 4^+ states and thus obviously

cannot be considered as enhancement factor. The size of this effect together with the dynamic effect of exciting these states in ^{54}Fe by a two-step reaction process can be estimated experimentally from the enhancement of the $J = 2$ cross section in ^{52}Fe as about 20–30 % so of the total cross section. The contribution of these processess for the strongly excited, isolated $f_{\frac{7}{2}}^n$ states which were used to extract εD_0^2 is then probably $\leqq 20\,\%$.

The experimental and theoretical enhancement factors are compared in table 3. It is interesting to investigate the enhancement factor due to a major shell alone. Considering only the fp configurations in table 8, the enhancement factors are 2.40, 1.50, 1.10 and 1.00 for $J = 0$–6, respectively. These values lead to an average D_0^2 of about 33 for $J = 0$–4, which is a typical value needed in the sd shell using complete $(sd)^n$ wave functions [12]). An analysis [21]) of the (t, p) reaction for $L = 0$ transfers over the entire periodic table using complete major shell wave functions yielded a similar average D_0^2 value (≈ 32). For $J = 0$ the enhancement factor would be 7.86 for the sum rule [21]) $[\sigma = \sum_{j'} \sigma(j'^2)]$ which means that only about 30 % of the fp shell sum rule is exhausted in the ^{54}Fe ground state.

Finally the enhancement factors were calculated with all of the sd-fp-$g_{\frac{9}{2}}$ components given in table 8, and an average value of $D_0^2 = 20$ was obtained for $J = 0$–6. This still large value of D_0^2 can originate from the approximations made in the zero-range DWBA calculation as well as from the neglect of additional pair correlation effects from orbitals further from the Fermi surface [23]). An important phenomenological question is how many orbits need to be considered so that D_0^2 is independent of L. From table 3 it appears that a major shell is probably not sufficient in this case since much of the $J = 0$ and 2 enhancement comes from the sd shell.

In this mass region the $L = 6$ pickup is the least affected of the L-values by configuration mixing. However, it is difficult to extract a believable enhancement factor in this case because the $L = 6$ angular distributions are badly fitted by the zero-range DWBA. Because of the simple shell model structure for the $L = 6$ pickup especially for the two lowest $T = 1$ states it would be very instructive to carry out finite-range DWBA calculations to attempt to explain the angular distributions and the enhancement factor for these states.

5. Conclusions

The lack of wave functions for the ^{54}Fe and ^{52}Fe nuclei calculated in a full fp shell model space does not allow a detailed comparison between theory and experiment. However, the $f_{\frac{7}{2}}$ shell calculations presented do describe reasonably well the strongest positive parity states, especially for the states with low spin. The 2p-2h admixtures to the $f_{\frac{7}{2}}$ wave functions calculated in perturbation theory explain successfully the strong enhancement of $L = 0$ transitions as well as the smaller enhancement of the $L = 2$ and 4 transitions. Zero-range DWBA calculations do not reproduce in a

satisfactory way the transitions with higher L-values and cannot account for the variety of angular distribution shapes.

One of the authors (P.D.) would like to express his appreciation for hospitality of the Cyclotron Laboratory staff during his stay at Michigan State University.

References

1) W. Bohne, H. Fuchs, K. Grabisch, D. Hilscher, U. Jahnke, H. Kluge, T. G. Masterson and H. Morgenstern, Nucl. Phys. **A245** (1975) 107
2) D. Evers, W. Assmann, K. Rudolph and S. J. Skorka, Nucl. Phys. **A198** (1972) 268
3) J. B. Viano, Y. Dupont and J. Menet, Phys. Lett. **34B** (1971) 397
4) T. Suehiro, Y. Ishizaki, H. Ogata, J. Kokane, Y. Saji, A. Stricker, Y. Sugiama and I. Nonaka, Phys. Lett. **33B** (1970) 468
5) G. Bassani, N. M. Hintz and C. D. Kavaloski, Phys. Rev. **136** (1964) B1006
6) G. T. Garvey, J. Cerny and R. H. Pehl, Phys. Rev. Lett. **12** (1964) 726
7) R. G. Markham and R. G. H. Robertson, Nucl. Instr. **129** (1975) 131
8) F. D. Becchetti and G. W. Greenlees, Phys. Rev. **182** (1968) 1190
9) A. Guichard, W. Benenson and H. Nann, Phys. Rev. **C11** (1975) 2027
10) A. Moalem, M. A. M. Shahabuddin, R. G. Markham and H. Nann, Phys. Lett. **58B** (1975) 286
11) A. Saha and H. Nann, unpublished
12) H. Nann and B. H. Wildenthal, Phys. Rev. **C13** (1976) 1009
13) H. W. Baer, J. J. Kraushaar, C. E. Moss, N. S. P. King, R. E. L. Green, P. D. Kunz and E. Rost, Ann. of Phys. **76** (1973) 437
14) W. Kutschera, B. A. Brown and K. Ogawa, Nuovo Cim., submitted
15) D. F. Geesaman, R. Malmin, R. L. McGrath, J. W. Noé and J. Cerny, Phys. Rev. Lett. **34** (1975) 326
16) B. A. Brown, D. B. Fossan, J. M. McDonald and K. A. Snover, Phys. Rev. **C9** (1974) 1033
17) R. F. Casten, E. R. Flynn, O. Hansen and J. T. Mulligan, Phys. Rev. **C4** (1974) 130;
B. F. Bayman and C. F. Clement, Phys. Rev. Lett. **29** (1969) 1020
18) S. M. Smith, P. G. Roos, A. M. Bernstein and C. Moazed, Nucl. Phys. **A158** (1970) 497
19) A. Bohr and B. R. Mottelson, Nuclear structure, vol. 2 (Benjamin, Reading, Massachusetts, 1975) p. 641
20) M. Harvey and F. C. Khanna, Nucl. Phys. **A221** (1974) 77
21) R. A. Broglia, C. Riedel and T. Udagawa, Nucl. Phys. **A184** (1973) 23
22) E. R. Flynn and O. Hansen, Phys. Lett. **31B** (1970) 135
23) R. A. Broglia, K. Kolltveit and B. Nilsson, Phys. Lett. **37B** (1971) 441